Orbital
The electronic journal of chemistry

the electronic journal of chemistry

Full Paper | http://dx.doi.org/10.17807/orbital.v17i2.21045

Magnetic Ferrites Synthesized from Leclanché Exhausted Batteries for Heavy Metal Detection

Santiago Kosloski [a], Jarem Raul Garcia [a], and Alan Fernando Yoshiaki Matsushita* [a]

The pervasive presence of heavy metals in the environment poses significant health risks, necessitating the development of efficient and cost-effective detection methods. This study explores the use of MFe_2O_4-based nanocomposites, synthesized from exhausted Leclanché cell residues, for the electrochemical detection of heavy metals such as Cu^{2+}, Hg^{2+}, Pb^{2+}, and Sn^{2+}. The nanocomposites were modified with silica (SiO_2) using tetraethyl orthosilicate (TEOS) to enhance their functional properties, particularly for improved stability and surface functionality crucial for environmental applications. Comprehensive characterization techniques including XRD, FTIR, SEM, TEM, and DLS confirmed the successful synthesis and modification of the nanoparticles. Electrochemical assessments demonstrated the nanocomposites capability to detect heavy metals with good sensitivity, validated through Differential Pulse Stripping Voltammetry (DPSV). This preliminary study not only proves the efficacy of $MFe_2O_4@SiO_2$ in detecting individual heavy metals but also sets the groundwork for future research on their application in real-world environmental samples and mixed-metal scenarios. The advancement of such nanotechnology-based sensors represents a promising approach to enhancing public health and environmental safety protocols.

Graphical abstract

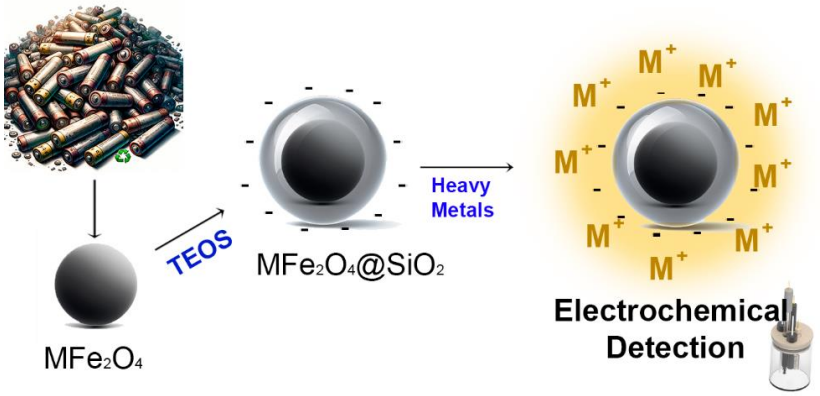

Keywords

Electrochemical sensors
Heavy metal detection
MFe_2O_4
SiO_2 modification

Article history

Received 01 may 2024
Revised 23 Jul 2024
Accepted 30 Mar 2025
Available online 18 May 2025

Handling Editor: Sergio R. Lazaro

1. Introduction

The detection of heavy metals in the environment is a critical area of study due to the significant health risks these elements pose to both ecosystems and human populations. Heavy metals such as lead, mercury, and arsenic, are persistent environmental pollutants that can accumulate in biological systems, leading to toxic effects even at low concentrations [1–3]. Chronic exposure to heavy metals has been linked to a range of health issues including neurological disorders, renal dysfunction, and cancer, underscoring the necessity for effective monitoring and remediation strategies [4]. Accurate and sensitive detection methods are essential for assessing the extent of pollution and for initiating

[a] Departament of Chemistry, State University of Ponta Grossa (UEPG). Av. Gal. Carlos Cavalcanti, 4748 – Uvaranas, Ponta Grossa, PR, Brazil, 84030-900. *Corresponding author. E-mail: **alanmatsushita@hotmail.com**

appropriate environmental protection measures. Moreover, the monitoring of these contaminants aids in enforcing environmental regulations and in the development of new policies to mitigate the release of hazardous substances into the environment [5–7]. As such, the advancement of analytical techniques for the detection of heavy metals is not only relevant for environmental science but also critical for public health and safety.

Numerous conventional methods are employed for the detection of heavy metals, including Energy Dispersive X-ray Spectroscopy (EDX), ICP-MS, fluorescence spectroscopy, and other sophisticated analytical techniques [8–10]. While these methods are known for their accuracy and reliability, they are often expensive and time-consuming, frequently requiring complex sample preparation steps. As a result, there is a significant demand for the development of rapid and precise methods to identify heavy metals. Developing such methods is of extreme importance, not only to reduce the costs associated with heavy metal detection but also to facilitate quicker decision-making processes in environmental monitoring and public health protection. The ability to rapidly identify and quantify heavy metals can lead to more immediate responses to pollution incidents and help in the enforcement of environmental regulations, thereby minimizing the long-term environmental and health impacts of these hazardous substances.

Electrochemical detection techniques offer significant advantages for the identification of contaminants due to their high sensitivity and low operational costs. These methods not only allow for the precise quantification of trace levels of substances but also offer flexibility in electrode material selection, which can be tailored to detect a wide range of analytes. This adaptability enhances the utility of electrochemical sensors in various applications, from environmental monitoring to medical diagnostics [11,12] . Furthermore, the ability to use different materials for electrodes can lead to the development of customized sensors that are specifically designed for targets, making electrochemical detection a highly effective approach in the field of analytical chemistry. As such, these electrodes are invaluable tools for rapid and efficient detection, providing essential data that supports environmental protection and public health initiatives.

Magnetic nanoferrites, particularly MFe_2O_4 (M=Metal), have garnered considerable attention in the field of electrochemical detection due to their distinctive properties [13,14]. These include chemical stability and easy recoverability via magnetic susceptibility, among others, which endow them with significant potential for analytical applications. The inherent stability of MFe_2O_4 ensures that the material remains intact under a variety of environmental conditions, while its magnetic properties allow for straightforward separation processes, enhancing the practicality of its use in continuous monitoring systems.

In this study, magnetic nanoferrites were synthesized from exhausted Leclanché cell residues. This approach not only promotes the recycling of waste materials but also contributes to the development of cost-effective and environmentally friendly sensors. While previous studies [15–18], have explored obtaining materials from spent Leclanché batteries, our work differs in several innovative aspects. Firstly, our research not only synthesizes MFe_2O_4 (M = Mn, Co, Ni, Zn) nanoferrites from battery residues but also modifies these nanomaterials with tetraethyl orthosilicate (TEOS), resulting in $MFe_2O_4@SiO_2$ nanocomposites. This modification with TEOS provides greater stability and surface functionality to the nanocomposites, which are crucial for environmental applications [19]. Additionally, a significant distinction of our approach is that we do not adjust the concentrations of metals in the solution; we use the solution as obtained from the spent batteries. This simplified method is advantageous as it reduces the need for additional purification and concentration adjustment processes, making the procedure more efficient and sustainable. The synthesized nanocomposites were thoroughly characterized using techniques such as X-ray diffraction (XRD), Fourier-transform infrared spectroscopy (FTIR), scanning electron microscopy (SEM), transmission electron microscopy (TEM), and dynamic light scattering (DLS). Subsequently, these materials were employed in glassy carbon electrodes for the detection of heavy metals, including Cu^{2+}, Hg^{2+}, Pb^{2+} and Sn^{2+}. The electrochemical testing conducted demonstrated the successful synthesis of the nanocomposites and their capability to effectively identify these metals. The results highlight the potential of using MFe_2O_4-based nanocomposites in electrochemical sensors, offering a promising route for the development of advanced tools for environmental monitoring and pollution control.

2. Material and Methods

2.1 Chemical Materials

All chemicals were commercially available and used without further purification. Sodium hydroxide (NaOH), sulfuric acid (H_2SO_4), Tetraethyl orthosilicate (TEOS), Aqueous Ammonia (25%) and Lead(II) chloride ($PbCl_2$) were purchased from Sigma -Aldrich. Copper chloride ($CuCl_2$), Tin(II) Chloride ($SnCl_2$) were purchased Synth company. Mercury(II) Chloride ($HgCl_2$), Acetic acid, Sodium acetate and Citric Acid were purchased from Fluka. 1 M acetate buffer solution (pH = 5) was prepared by mixing 1 M acetic acid and 1 M sodium acetate.Milli - Q water was used throughout all experiments.

2.2 Dismantling of exhausted Leclanché batteries.

Ten exhausted Leclanché batteries were disassembled for this study. In this process, the metallic casing of the battery was separated from the paste obtained from the inner part of the battery. The metallic casing was dissolved in 4 $mol.L^{-1}$ sulfuric acid and left to rest for 3 days. The paste obtained from inside the battery was calcined at 400 degrees Celsius. These materials were obtained to serve as precursors for ferrites.

2.3 Preparation of MFe_2O_4 and $MFe_2O_4@SiO_2$

The ferrites, MFe_2O_4 (M = Mn, Co, Ni, Zn), were synthesized using a hydrothermal method. The synthesis was conducted by adding 0.5g of the paste obtained from the battery, 0.4g of citric acid, and 10 mL of the Fe^{2+} solution obtained by dissolving the battery casing in sulfuric acid. To this solution, 15 mL of a 1 $mol.L^{-1}$ NaOH solution was added before transferring it into a Teflon-lined stainless-steel autoclave maintained at 90 °C for 2 hours. After cooling the autoclave to room temperature (25°C), the resulting MFe2O4 nanoparticles (NPs) were washed three times with ethanol and ultrapure water and subsequently dried in a vacuum oven at 50°C.

The obtained MFe_2O_4 nanoparticles were modified with silica to introduce hydroxide groups on their surface using a well-established method from the literature[20]. Initially, 500 mg of MFe_2O_4 was added to a solution of ethanol/water (5:1)

under ultrasonic bath treatment for 30 minutes. Subsequently, 10 mL of 25% (v/v) aqueous ammonia and 4 mL of TEOS were added. The mixture was stirred for 4 hours at room temperature. Finally, the resulting product, $MFe_2O_4@SiO_2$, was washed with ethanol and ultrapure water to neutralize it and then dried in a vacuum oven at 50°C.

2.4 Characterization

The X-ray diffraction patterns of the synthesized materials were determined by a Rigaku Ultima IV diffractometer using CuKα radiation (λ = 1.5406 Å) operated at 40 kV/30 mA. The diffraction patterns were recorded using 0.02° per step and 1° min^{-1} in the range 5° < 2θ < 75°.

The Zeta Potential were assisted by Zetasizer Nano-Zs90–Nanoseries.

Attenuated reflection infrared spectroscopy (ATR-FTIR) was performed in a Shimadzu / IRPrestige-21Spectrometer, with wavenumber ranging from 400 to 4000 cm^{-1}. High Resolution Scanning Electronic Microscopy (HR-SEM) micrographs were obtained using a Tescan Mira 3 scanning electron microscope, operating under low vacuum at 2kV. Elemental analysis on microscopic sections of composites was performed by Energy Dispersive Spectroscopy – Tescan. The particles size was also evaluated by transmission electron microscopy in low resolution mode and that was performed in the JEOL JEM 1200 equipment

The elemental analysis of the materials was carried out by Rigaku/ZSX Primus II, XRF spectroscopy.

2.5 Preparation of $MFe_2O_4@SiO_2$-based sensors

0.5 mg of $MFe_2O_4@SiO_2$ was suspended in 1000 µL of a 1 M NaOH aqueous solution and shaken for 10 minutes at 25°C. Subsequently, the $MFe_2O_4@SiO_2$ was separated using an external magnetic field. Next, different concentrations of metal ion solutions (Cu^{2+}, Hg^{2+}, Pb^{2+}, and Sn^{2+}) were mixed with the $MFe_2O_4@SiO_2$ and left in contact with the solution for 10 minutes. Afterward, $MFe_2O_4@SiO_2$-M^{2+} was separated by a magnet and mixed with 100 µL of ethanol. This solution then dropwise added to the surface of a glassy carbon electrode (GCE). After the GCE surface naturally dried at room temperature, electrochemical tests were conducted.

2.6 Electrochemical Measurements

The electrochemical characterization was performed in a three-electrode cell connected to a Potentiostat/Galvanostat Methrom Autolab model M204, equipped with electrochemical impedance module FRA32, using an Ag|AgCl (3 M) reference electrode and A platinum (Pt) foil with an area of 1 cm^2 was used as auxiliary electrode. The electrochemical performance was characterized using Differential Pulse Stripping Voltammetry (DPSV), and measurements were carried out with a quiet time of 10 seconds and a pulse width of 0.2 seconds, a potential range of -1.0 V-+0.4 V, an amplitude of 50 mV, and a potential increment of 5 mV. For all electrochemical measurements, the support electrolyte used was acetate buffer solution.

3. Results and Discussion

3.1 Synthesis and Characterization of MFe_2O_4 and $MFe_2O_4@SiO_2$

The XRF analysis of the paste extracted from the batteries revealed a composition primarily consisting of Mn (44.2 wt%) and Zn (21.2 wt%), along with various other metals in smaller quantities. The values are presented in Table 1.

Table 1. Elemental Composition of Battery Paste by XRF Analysis.

No.	Component	Result	Unit	Det. limit	El. line
1	C	1.40	mass%	0.31905	C -KA
2	O	27.6	mass%	0.88355	O -KA
3	Mg	0.106	mass%	0.06017	Mg-KA
4	Al	1.71	mass%	0.07612	Al-KA
5	Si	0.488	mass%	0.00896	Si-KA
6	P	0.0114	mass%	0.00395	P -KA
7	S	0.465	mass%	0.00586	S -KA
8	Cl	2.20	mass%	0.03372	Cl-KA
9	Ca	0.162	mass%	0.00947	Ca-KA
10	Mn	44.2	mass%	0.04402	Mn-KA
11	Fe	0.414	mass%	0.02925	Fe-KA
12	Ni	0.0447	mass%	0.01094	Ni-KA
13	Zn	21.2	mass%	0.02202	Zn-KA

This mixture was successfully used to synthesize MFe_2O_4 ferrites, which were subsequently modified with TEOS to enhance their functional properties and potential applications. This modification process was designed to leverage the unique characteristics of SiO_2, such as improved stability and surface functionalization.

The X-ray diffraction patterns of the obtained nanoparticles, MFe_2O_4 and $MFe_2O_4@SiO_2$, are presented in Figure 1. The identified diffraction peaks were in excellent agreement with the standard JCPDS cards for $MnFe_2O_4$ [22-1088] and $ZnFe_2O_4$ [22-1012], confirming the formation of a single-phase spinel structure. The observed peaks at 2θ

values of 18.14°, 30.2°, 35.4°, 37.27°, 42.82°, 53.21°, 56.73°, and 62.15° corresponded to the (111), (220), (311), (222), (400), (422), (511), and (440) planes, respectively [21].

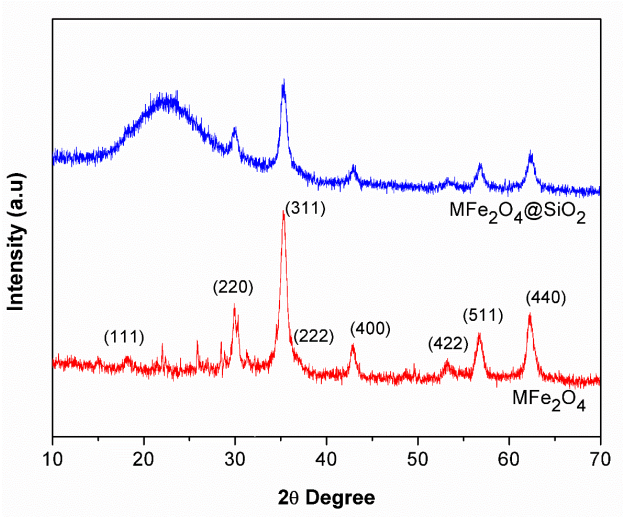

Fig. 1. Powder X-ray diffraction pattern of simple ferrites MFe_2O_4 (M = Mn and Zn).

However, it is worth noting that in the X-ray diffraction (XRD) pattern of MFe_2O_4@SiO_2, a distinct feature was observed. While most of the diffraction peaks corresponded to the expected crystalline phases of $MnFe_2O_4$ and $ZnFe_2O_4$, there was an additional broad hump in the XRD pattern, indicative of an amorphous component. This amorphous feature, observed at [18~30 2θ], suggests that the nanoparticles were coated with a layer of SiO_2. Importantly, this amorphous characteristic does not affect the crystalline structure of the nanoparticles, as no peaks related to SiO_2 were observed in the XRD pattern of the nanostructures [22,23].

The FTIR spectral analyses of MFe_2O_4 and MFe_2O_4@SiO_2 (Fig. 2) reveal significant changes in the spectral bands, indicative of the influence of SiO_2 incorporation. Notably, there is a shift in the peak at 410 cm^{-1}, corresponding to the M-O stretching vibration in the octahedral position, and the absorption band at 580 cm^{-1}, associated with the M-O stretching vibration in the tetrahedral position [24,25], both of which show marked shifts in the MFe_2O_4@SiO_2 samples compared to the pure ferrite. Additionally, new absorption bands unique to the MFe_2O_4@SiO_2 are identified at 1101 cm^{-1} and 801 cm^{-1}, attributed to Si-O-Si bonds, at 947 cm^{-1} corresponding to Si-OH groups, and at 470 cm^{-1} associated with Si-O. These bands confirm the presence of SiO_2 on the surface of the ferrites and are indicative of specific interactions between silica and the functional groups present in the ferrites, contributing to the modification of the materials surface properties [26, 27].

SEM images of MFe_2O_4 and MFe_2O_4@SiO_2, along with their corresponding energy-dispersive X-ray spectroscopy (EDS) spectra, are presented in Figure 3. Figures 3a and 3b depict MFe_2O_4 as small, well-defined grains with a broad size distribution ranging approximately from 40 to 120 nm. In contrast, the MFe_2O_4@SiO_2 (Figures 3d and 3e) exhibits a smooth and monodisperse morphology with an average size of 800 nm after the silica microspheres have coated the MFe_2O_4, maintaining a spherical morphology consistent with SiO_2 spheres. The EDS results for MFe_2O_4 and MFe_2O_4@SiO_2 are displayed in Figures 3c and 3f, respectively. The EDS analysis crucially highlights the presence of increased Si concentration in the MFe_2O_4@SiO_2. This enhancement can be attributed to the silica coating derived from the TEOS, which effectively encapsulates the magnetic core.

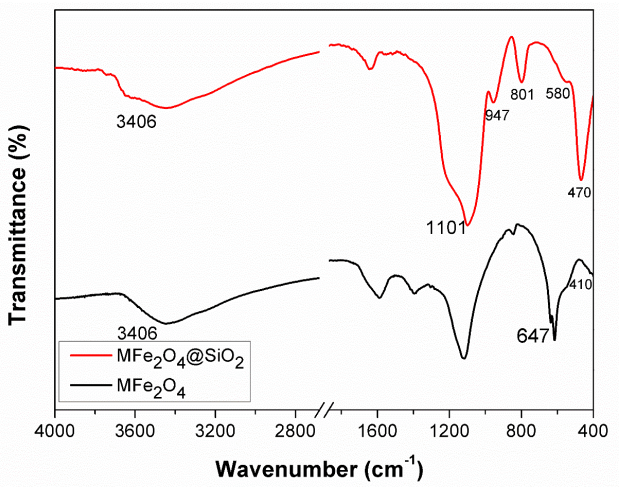

Fig. 2. FTIR spectra of pure MFe_2O_4 and MFe_2O_4@SiO_2 (TEOS coated).

For the synthesized ferrites, the elemental mapping conducted by EDS (Figure 4) revealed distinct characteristics. The MFe_2O_4 ferrite exhibits homogeneity with a uniform distribution of elements. In contrast, the MFe_2O_4@SiO_2 ferrite shows a significant increase in the presence of silicon (Si) and oxygen (O) elements, indicating a successful encapsulation of MFe_2O_4 particles by SiO_2. This encapsulation suggests enhanced stability and functionality of the nanoparticles, especially in environments where chemical reactivity is critical.

TEM Micrographs of MFe_2O_4 and MFe_2O_4@SiO_2 are presented in Figure 5. This analysis revealed that MFe_2O_4 consists of cube-like shape nanoparticles with varying size distributions and a tendency to agglomerate. The agglomeration can be attributed to the zeta potential of 8.82 mV, which indicates moderate stability and a propensity for particle agglomeration due to insufficient electrostatic repulsion. In contrast, MFe_2O_4@SiO_2 nanoparticles exhibit a more spherical shape and larger dimensions, corroborating the observations made in SEM analyses.

The modification of MFe_2O_4 with SiO_2 changes the surface properties and consequently enhances the functionality of these nanoparticles [28]. The modification with SiO_2 enhances the surface charge, resulting in a zeta potential of -60.3 mV, which significantly improves the colloidal stability and reduces the tendency to agglomerate. These findings are critical as they offer insights into the stability and behavior of the nanoparticles in aqueous solutions. Notably, the more negative zeta potential observed for MFe_2O_4@SiO_2 typically improves the stability of colloidal systems and enhances the nanoparticles capacity to interact with and bind heavy metals in solution [29]. The increased negative charge facilitates stronger electrostatic interactions with positively charged metal ions, thereby aiding the adsorption process.

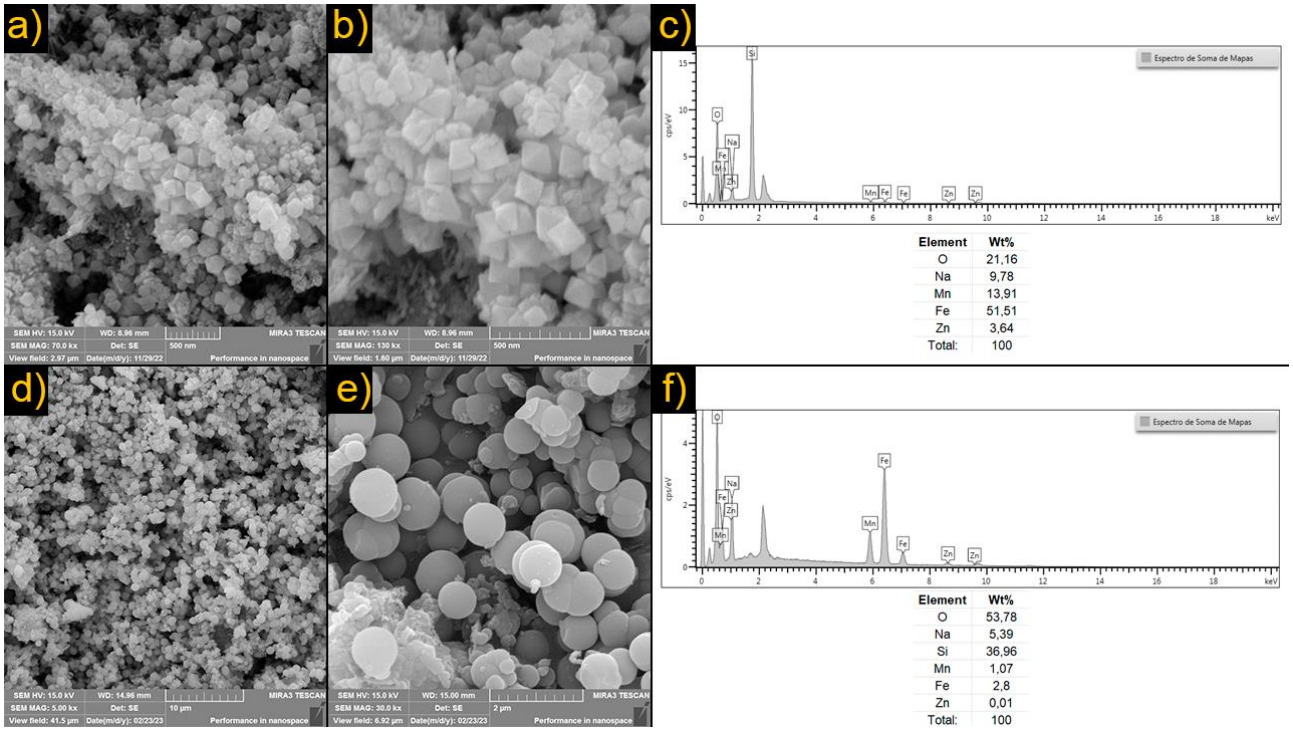

Fig. 3. SEM Images and EDS Spectra of Nanoparticles: SEM images of MFe_2O_4 shown in panels (a, b), and MFe_2O_4@SiO_2 in panels (d, e). EDS spectra for MFe_2O_4 and MFe_2O_4@SiO_2 are presented in panels (c) and (f), respectively.

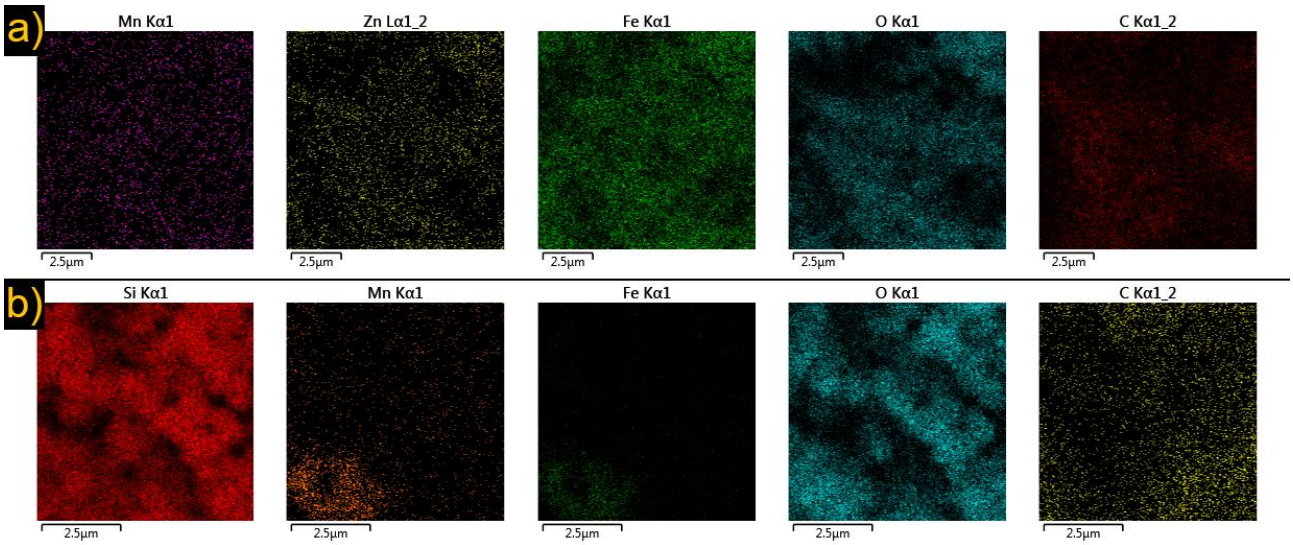

Fig. 4. EDS mapping of a) MFe_2O_4 and b) MFe_2O_4@SiO_2.

3.2 Detection of Heavy Metal ions (Cu2+, Hg2+, Pb2+ and Sn2+)

To assess the applicability of these nanoparticles, tests were conducted using the obtained MFe_2O_4@SiO_2, which exhibited negative charges as evidenced by the zeta potential measurements. The nanoparticles were tested using Differential Pulse Stripping Voltammetry (DPSV) technique, with the results displayed in Figure 6. During these tests, varying concentrations of metals (Cu^{2+}, Hg^{2+}, Pb^{2+}, and Sn^{2+}) were introduced, revealing that the current peaks increased proportionally with the concentrations of these metals in the studied range (0.5 – 10.5 µM). This preliminary test indicated that the synthesized MFe_2O_4@SiO_2 nanocomposite could be effectively applied for the determination of heavy metals individually, demonstrating good sensitivity.

However, a more detailed study will be conducted to determine the performance of this nanocomposite in real sample matrices and with mixed metal solutions. Such studies are crucial to further validate the efficacy and robustness of the MFe_2O_4@SiO_2 nanocomposite in practical environmental applications, particularly in scenarios where complex metal mixtures pose a significant challenge. This will also help in understanding the interaction dynamics between mixed metals and the nanocomposite, aiming to optimize its use in widespread environmental monitoring and pollution control strategies.

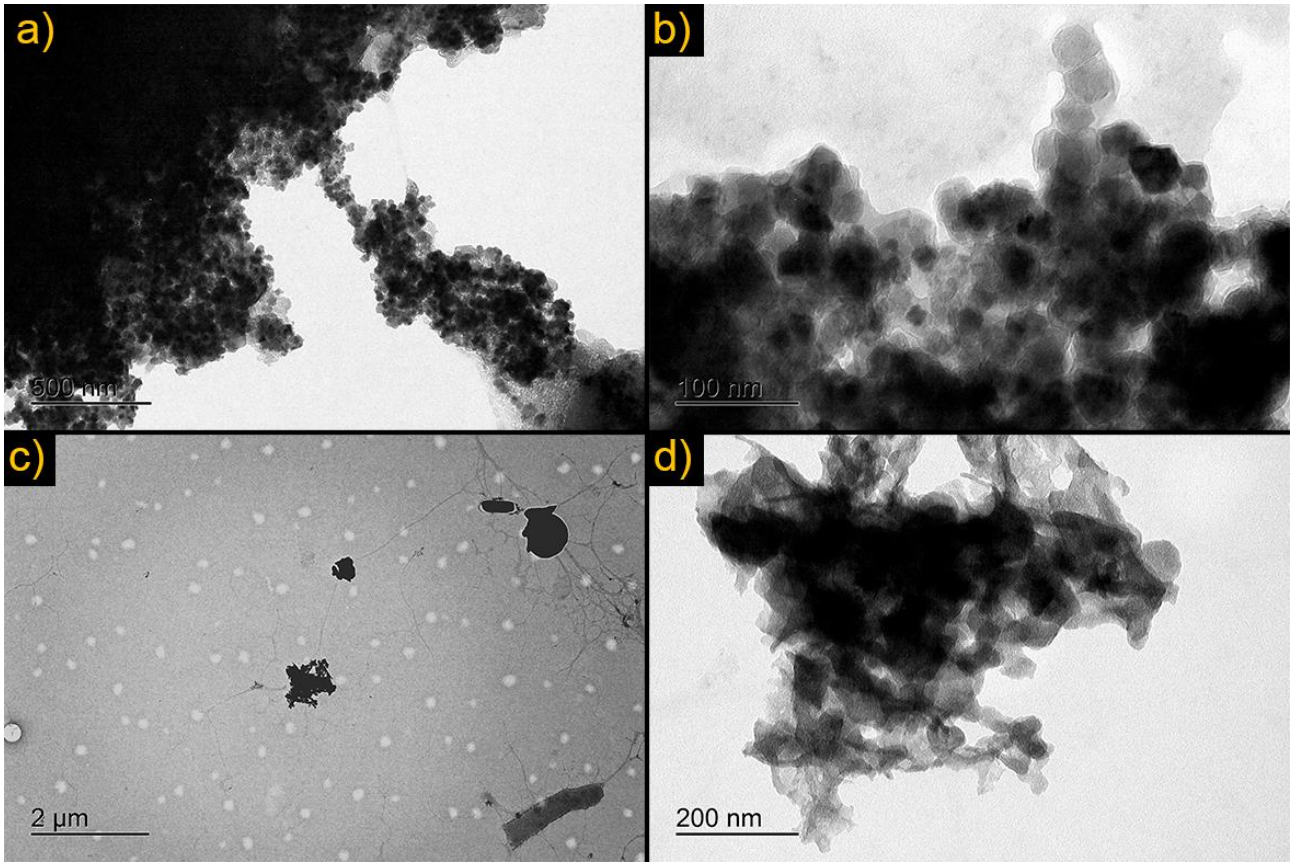

Fig. 5. TEM Micrographs of MFe_2O_4 shown in panels (a, b), and $MFe_2O_4@SiO_2$ in panels (c, d).

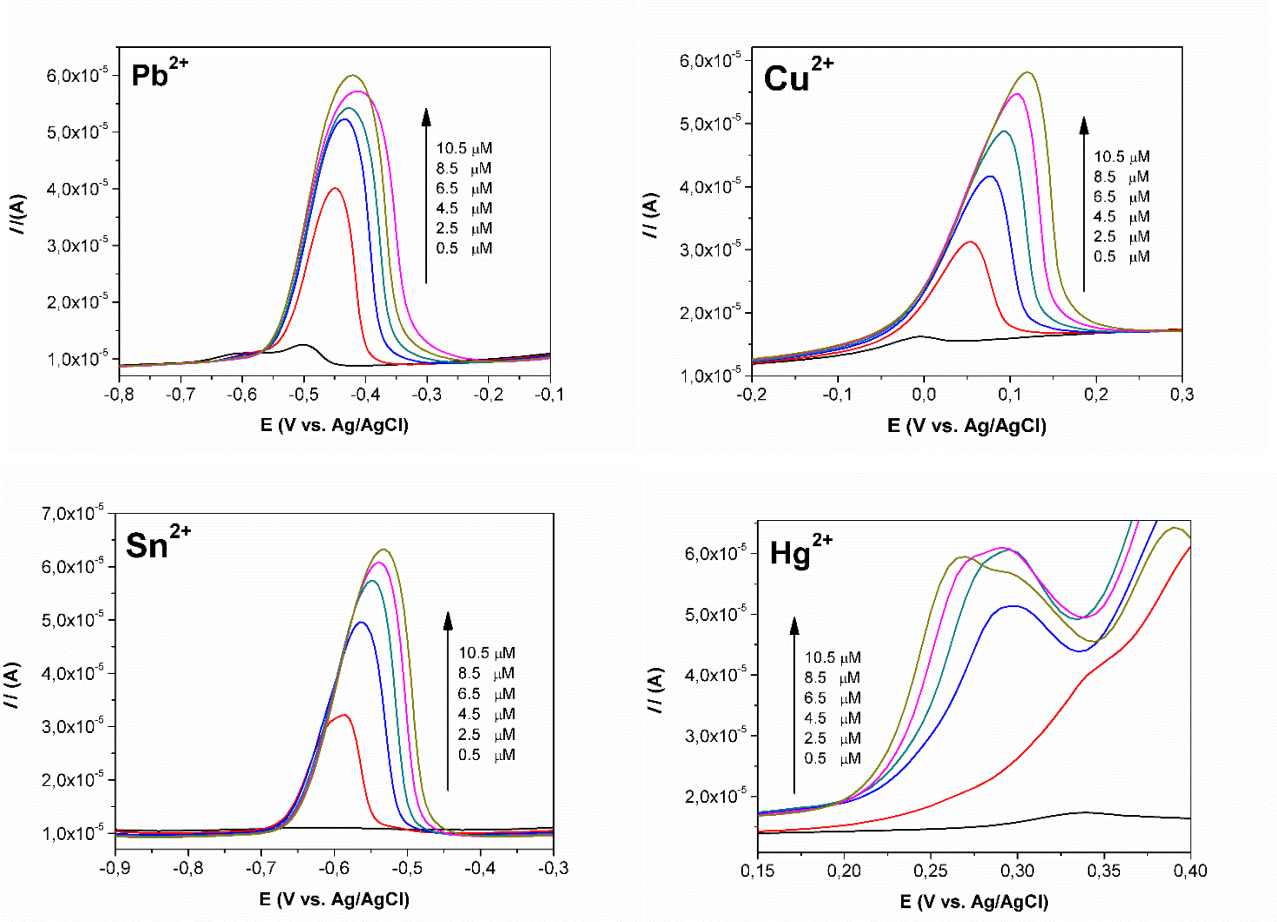

Fig. 6. DPSV curves of the $MFe_2O_4@SiO_2$ nanocomposite toward individual determination of (Cu^{2+}, Hg^{2+}, Pb^{2+}, and Sn^{2+}) ions at different concentrations.

4. Conclusions

In summary, this study successfully demonstrated the efficacy of MFe_2O_4-based nanocomposites, synthesized from exhausted Leclanché cell residues and modified with SiO_2, as a good candidate for electrochemical sensors for detecting heavy metals in aqueous solutions. The comprehensive characterization of these nanocomposites confirmed their enhanced stability and surface functionality, critical for sensitive and reliable detection. The promising results from Differential Pulse Stripping Voltammetry (DPSV) tests, showed clear correlations between metal ion concentrations and current responses, highlight the potential of these materials in environmental monitoring. Future research will focus on expanding the application of these sensors to real sample matrices and mixed-metal scenarios, further refining their sensitivity and selectivity. This work contributes significantly to environmental protection efforts, underscoring the importance of developing sustainable and cost-effective technologies for public health and safety.

Acknowledgments

A.F.Y.M. acknowledges the financial support provided by the Conselho Nacional de Desenvolvimento Científico e Tecnológico (CNPq – Brazil) – Post-PhD research grant (Grant number 151838/2022-4).

Author Contributions

Alan F.Y. Matsushita: Conceptualization, Data curation, Formal analysis, Investigation, Methodology, Validation, Writing – original draft. Santiago Kosloski: Data curation, Formal analysis, Methodology, Data curation, Validation, Writing – original draft. Jarem R. Garcia: Conceptualization, Data curation, Formal analysis, Funding acquisition, Investigation, Methodology, Resources, Supervision, Validation, Visualization, Writing – original draft, Writing – review & editing.

References and Notes

[1] Khan, F. S. A.; Mubarak, N. M.; Tan, Y. H.; Khalid, M.; Karri, R. R.; Walvekar, R.; Abdullah, E. C.; Nizamuddin, S.; Mazari, S. A. *J. Hazard Mater*. **2021**, *413*, 125375. [Crossref]

[2] Sun, F.; Mu, Y.; Leung, K. M. Y.; Su, H.; Wu, F. *H. Environ. Sci. Policy* **2021**, *124*, 413. [Crossref]

[3] Zhou, X. *Int. J. Electrochem. Sci.* **2024**, *19*, 100559. [Crossref]

[4] Zahir, F.; Rizwi, S. J.; Haq, S. Q.; Khan, R. H. Environ. Toxicol. Pharmacol. 2005, 20, 351. [Crossref]

[5] Zhang, Y.; Liao, Y.; Yin, X.; Zhang, Y.; Yang, Z.; Wang, H.; Yang, W.; Pang, P. *Microchem. J.* **2023**,*189*, 108544. [Crossref]

[6] Elsebai, B.; Ghica, M. E.; Abbas, M. N.; Brett, C. M. A. *Molecules* **2023**, *28*, 2809. [Crossref]

[7] Gao, J.; Yin, J.; Wang, G.; Wang, X.; Zhang, J.; Sun, B.; He, D.; Suo, H.; Zhao, C. *Food Chem*. **2024**, *448*, 138994. [Crossref]

[8] Chen, W.; Yang, Y.; Fu, K.; Zhang, D.; Wang, Z. *Front. Pharmacol*. **2022**, *13*, 891273. [Crossref]

[9] Matsushita, A. F. Y.; Tapia, M. J.; Pais, A. A. C. C.; Valente, A. J. M. *Polymers (Basel)* **2020**, *12*, 1314. [Crossref]

[10] Bhuvaneswari, K.; Radha, S.; Sreeja, B. S.; Kumar, P. S. *Environ. Res.* **2023**, *225*, 115570. [Crossref]

[11] Li, B.; Xie, X.; Meng, T.; Guo, X.; Li, Q.; Yang, Y.; Jin, H.; Jin, C.; Meng, X.; Pang, H. *Food Chem*. **2024**, *440*, 138213. [Crossref]

[12] Zhang, M.; Guo, W. Food Chem. 2023, 406, 135034. [Crossref]

[13] Vicente-Martínez, Y.; Arroniz-Lázaro, A.; Hernández-Córdoba, M.; López-García, I. *Green Anal. Chem*. **2024**, *8*, 100089. [Crossref]

[14] Divakara, S. G.; Mahesh, B. *Results Eng.* **2024**, *21*, 101702. [Crossref]

[15] Xi, G.; Yang, L.; Lu, M. *Mater. Lett.* **2006**, *60*, 3582. [Crossref]

[16] Nan, J.; Han, D.; Cui, M.; Yang, M.; Pan, L. *J. Hazard Mater.* **2006**, *133*, 257. [Crossref]

[17] Kim, T. H.; Senanayake, G.; Kang, J. G.; Sohn, J. S.; Rhee, K. I.; Lee, S. W.; Shin, S. M. *Hydrometallurgy* **2009**, *96*, 154. [Crossref]

[18] Xi, G.; Li, Y.; Liu, Y. *Mater. Lett*. **2004**, *58*, 1164. [Crossref]

[19] Alimunnisa, J.; Ravichandran, J.; Meena, K. S. *J. Mol. Liq*. **2017**, *231*, 281. [Crossref]

[20] Dinali, L. A. F.; de Oliveira, H. L.; Teixeira, L. S.; da Silva, A. T. M.; D'Oliveira, K. A.; Cuin, A.; Borges, K. B. *Microchem. J.* **2020**, *154*, 104648. [Crossref]

[21] Yetim, N. K.; Baysak, F. K.; Koç, M. M.; Nartop, D. *J. Mater. Sci.:Mater. Electron.* **2020**, *31*, 18278. [Crossref]

[22] Zarei, A.; Saedi, S.; Seidi, F. *J. Inorg. Organomet. Polym. Mater*. **2018**, *28*, 2835. [Crossref]

[23] Mirzabe, G. H.; Keshtkar, A. R. *J. Ind. Eng. Chem.* **2015**, *26*, 277. [Crossref]

[24] Huang, Z.; Gao, P.; Zheng, H.; Liu, X.; Wen, J.; Rebrov, E. V. *Ceram. Int*. **2019**, *45*, 15980. [Crossref]

[25] Prasad, S. A. V.; Deepty, M.; Ramesh, P. N.; Prasad, G.; Srinivasarao, K.; Srinivas, C.; Babu, K. V.; Kumar, E. R.; Mohan, N. K.; Sastry, D. L. *Ceram. Int*. **2018**, *44*, 10517. [Crossref]

[26] Liang, Y.; Ouyang, J.; Wang, H.; Wang, W.; Chui, P.; Sun, K. *Appl. Surf. Sci.* **2012**, *258*, 3689. [Crossref]

[27] Kumar, G. S.; Srinivasan, R.; Karunakaran, G.; Kolesnikov, E.; Kim, M.; Karpenkov, D. Y. *Applied Physics A* **2021**, *127*, 546. [Crossref]

[28] Yetim, N. K.; Baysak, F. K.; Koç, M. M.; Nartop, D. *J. Mater. Sci.:Mater. Electron.* **2020**, *31*, 18278. [Crossref]

[29] Wang, L.; Cheng, C.; Tapas, S.; Lei, J.; Matsuoka, M.; Zhang, J.; Zhang, F. *J. Mater. Chem. A Mater.* **2015**, *3*, 13357. [Crossref]

How to cite this article

Kosloski, S.; Garcia, J. R.; Matsushita, F. Y. *Orbital: Electronic J. Chem*. **2025**, *17*, 210. DOI: http://dx.doi.org/10.17807/orbital.v17i2.21045